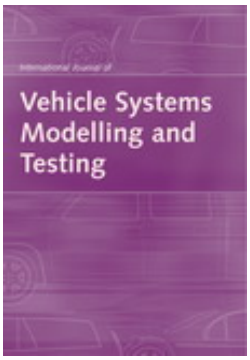

International Journal of Vehicle Systems Modelling and Testing

ISSN online: 1745-6444 - ISSN print: 1745-6436
https://www.inderscience.com/ijvsmt

Analysis of low frequency response characteristics of multi-inertia channel hydraulic mounts

Zhihong Lin

DOI: 10.1504/IJVSMT.2023.10058375

Article History:

Received:	04 August 2022
Last revised:	03 January 2023
Accepted:	25 February 2023
Published online:	20 August 2023

Analysis of low frequency response characteristics of multi-inertia channel hydraulic mounts

Zhihong Lin

School of Mechanical and Electrical Engineering,
Sanming University,
Sanming Fujian, 365004, China
Email: lin123hongzhi@163.com

Abstract: This paper investigates the effects of the number and length of inertia channels and different cross-sectional areas on the low-frequency characteristics of hydraulic mounts. Firstly, it analyses the isolation of low frequency-large amplitude excitation hydraulic mounts relying mainly on inertial channels. Secondly, nine different structures of inertia channels are proposed and the mathematical model of hydraulic mounts is obtained using an equivalent mechanical method. Finally, the hydraulic mounts system model of the 1/4 vehicle model is built to analyse the effect of different inertia channels on the mounts' vibration isolation performance under road excitation. It has been shown that changing the number of inertia channels as well as the cross-sectional area can regulate the peak and peak frequency of the dynamic stiffness and loss angle of the hydraulic mounts.

Keywords: hydraulic mounts; inertia channel; equivalent mechanical; 1/4 vehicle model; dynamic stiffness; loss angle.

Reference to this paper should be made as follows: Lin, Z. (2023) 'Analysis of low frequency response characteristics of multi-inertia channel hydraulic mounts', *Int. J. Vehicle Systems Modelling and Testing*, Vol. 17, No. 2, pp.143–163.

Biographical notes: Zhihong Lin has a PhD in Mechanical Engineering and is currently working at the School of Mechanical and Electrical Engineering, Sanming University, Fujian, China, where he is a pre-appointed Associate Professor. He graduated from Huaqiao University with a PhD in Mechanical Engineering. He received his MS in Marine and Offshore Engineering from Jimei University. His research interests include control, dynamics, and vehicle NVH.

1 Introduction

The engine mounts are vibration-isolating elements installed between the vehicle frame and the engine, which play an important role in improving the Noise, Vibration, and Harshness (NVH) of the vehicle. The desired properties of mounts include large stiffness and damping property under low-frequency large-amplitude excitation and small stiffness and damping under high-frequency small-amplitude excitation (Yu et al., 2001). The

analysis of the hydraulic mounts of single inertial channels and decoupler membrane channel combinations is now more mature. Singh et al. (1992) first derived a linear model of the inertial channel hydraulic mounts and analysed their dynamic characteristics. Tiwari et al. (2003) obtained the mathematical model for the combined hydraulic mounts of inertial channels and decoupler membrane channels by an experimental approach. Yoon and Singh (2010a, 2010b) proposed linear time-invariant, nonlinear and quasi-linear hydraulic mounts models and used the models to predict the transfer forces of hydraulic mounts under sinusoidal excitation conditions.

Studies on multi-inertia channel hydraulic mounts or bushings include the following. Zhang and Shangguan (2006) studied the effect of the number, size, and length of inertial channels on the low-frequency dynamic performance of hydraulic mounts. It is revealed that different numbers of inertia channels can change the stiffness and loss angle of hydraulic mounts vs. excitation frequency. Yang et al. (2016a, 2016b) studied the identification and mathematical modelling of the parameters of a multi-inertia channel hydraulic bushing system through an experimental approach. Then, the effect of inertia channel or orifice flow channel combination on the low-frequency dynamic characteristics of the hydraulic bushing was analysed. Chai et al. (2013, 2014, 2015) undertook mathematical modelling of hydraulic bushings with different combinations of inertial channels and orifice flow paths; next, the effects of different inertia channels and orifice flow paths on the dynamic and time-domain characteristics of the hydraulic bushings were analysed numerically and experimentally. Lu and Ari-Gur (2002) derived the set total parameter model of the hydraulic bushing with the number of inertia channels equal to 2 and performed the dynamic characteristics analysis. Lu et al. (2018) designed three structures of magnetorheological fluid mounts (8-holes, 16-holes, and slot); their studies have shown that 8 holes have better vibration isolation performance than 16 holes. Fan et al. (2020) proposed a semi-active hydraulic mount with four chambers and three flow channels. The semi-active mounts are characterised in two steps, the first step analyses the resonance caused by the long inertia channel, and the second step analyses the resonance caused by the shortest flow channel corresponding to the independent decoupler membrane (DM) fluid chamber. Finally, switching between these two cases allows the mounts to provide excellent NVH performance over a relatively wide band. Li et al. (2019) proposed a hydraulic mounts model with different inertia channel and hole combinations to optimise the inertia channel structural dimensions to obtain the best vibration isolation performance. Although studies on the time and frequency domain characteristics of multi-inertia channel hydraulic bushings have been reported, there are still some differences between hydraulic bushings and hydraulic mounts characteristics (Yang et al., 2016b; Lu and Ari-Gur, 2002; Barszcz et al., 2012).

Based on the above review, firstly, the inertial channel structural parameters directly affect the low-frequency dynamic characteristics of the hydraulic mounts based on the mathematical model of the inertial channel. Secondly, the hydraulic mounts for nine different combinations of inertia channels with different structures are proposed. Then, numerical analysis of the effects of the number, length, and cross-sectional area of the inertia channels is performed on the low-frequency dynamic characteristics of the hydraulic mounts. Finally, a 3-degree-of-freedom mounts system with a 1/4 vehicle model is built to analyse the effect of different inertia channel structures with low frequency-large amplitude on

the vibration isolation performance of the mounts. Numerical calculations show that changing the number, cross-sectional area, and length of inertia channels at low frequencies directly affects the low-frequency vibration isolation performance of hydraulic mounts.

2 Hydraulic mounts characteristics analysis

2.1 Hydraulic mounts with single inertia channel and decoupler membrane channel combination

Figure 1 shows the inertial channel combination decoupling membrane channel hydraulic mounts. Among them, Figure 1(a) shows the profile of the hydraulic mounts, and Figure 1(b) shows the lumped parameter model. The mounts are supported by the main spring rubber element providing a certain amount of stiffness and damping to support the weight of the static engine, denoted by K_r and B_r, respectively. When subjected to external excitation the fluid enters the lower chamber through the inertial and decoupler membrane channels, where the narrow inertial and decoupler membrane channels provide large damping for the mounts. where the flow rate through the inertial channel decoupler membrane channel is denoted by Q_i and Q_d, respectively; C_u and C_L are the compliance of the upper and lower chambers; P_1 and P_2 are the dynamic pressures of the upper and lower chambers, and A_p is the equivalent upper chamber cross-sectional area. Among them, the values of hydraulic mounts parameters are shown in Appendix.

Figure 1 Hydraulic mount: (a) profile diagram and (b) lumped parameter model (see online version for colours)

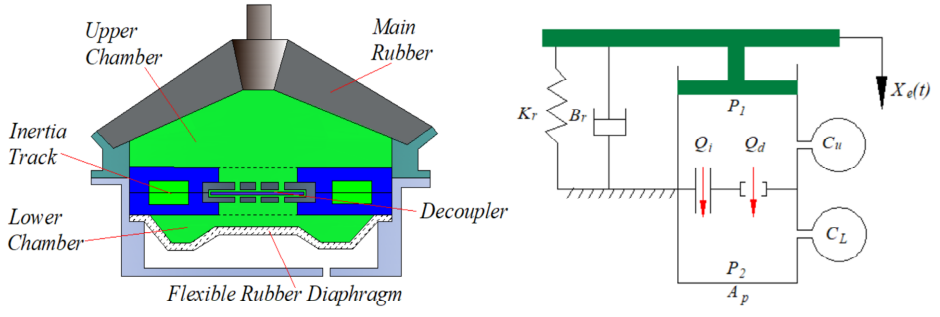

When the hydraulic suspension is excited by $X_e(t)$, the lumped parameter model of the hydraulic mounts can be solved according to Figure 1(b), see equations (1)–(3).

$$\begin{cases} P_1(t) - P_2(t) = I_i \dot{Q}_i(t) + R_i Q_i(t) \\ P_1(t) - P_2(t) = I_d \dot{Q}_d(t) + R_d Q_d(t) \end{cases} \tag{1}$$

$$\dot{P}_1(t) = \frac{A_p}{C_1} \dot{x}_e(t) - \frac{Q_i(t) + Q_d(t)}{C_1}, \dot{P}_2(t) = \frac{Q_i(t) + Q_d(t)}{C_2} \tag{2}$$

$$M\ddot{x}_e(t) + B_r\dot{x}_e(t) + K_r x_e(t) + A_p P_1(t) = 0 \tag{3}$$

where I_i and R_i are the inertia and resistance of the fluid passing through the inertial channel, and I_d and R_d are the inertia and resistance of the fluid passing through the decoupler membrane channel.

According to equations (1)–(3), the variation of the flow rate and amplitude A = 3 mm for frequency f = 5Hz and A = 1.5 mm for frequency f = 15 Hz were obtained, respectively, as shown in Figure 2. As can be seen from Figure 2, the flow through the decoupler membrane channel is negligible at low-frequencies with large amplitudes. Therefore, the effect of the decoupler membrane channel on the hydraulic mounts at low frequency-large amplitude excitation is negligible, which is the same conclusion as in the paper (Li et al., 2019).

Figure 2 Flow through inertial channel and decoupler membrane channel: (a) f = 5 Hz, A = 3 mm (b) f = 15 Hz, A = 1.5 mm (see online version for colours)

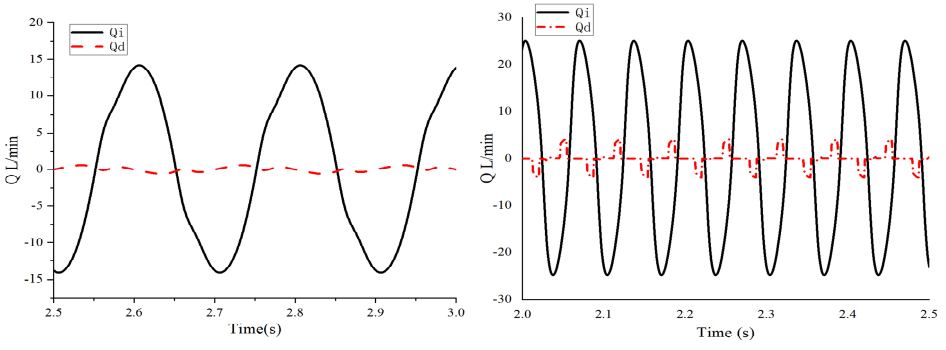

(a) (b)

2.2 *Effect of structural parameters of inertia channel on dynamic characteristics of hydraulic mounts*

Figures 3 and 4 show the effect of varying the equivalent cross-sectional area A_i and length L of the inertia channel on the dynamic characteristics of the hydraulic mounts, respectively. As can be seen from Figure 3, the respective peak and peak frequencies of the dynamic stiffness and loss angle of the hydraulic mounts increase with the increase of the equivalent cross-sectional area of the inertia channel. The respective peak and peak frequencies of the dynamic stiffness and loss angle of the hydraulic mounts decrease as the inertia channel length L increases. It follows that the cross-sectional area A_i of the inertia channel and the length L directly affect the dynamic stiffness and loss angle of the hydraulic mounts.

2.3 *Multiple structure hydraulic mounts inertia channel design*

In order to study the effects of variations in the number, length, and cross-sectional area of inertia channels on the low-frequency characteristics of hydraulic mounts. Table 1 and the nine inertia channel structures shown in Figure 5(a)–(i) are proposed.

Figure 3 Effect of equivalent cross-sectional area of inertia channel a_i on hydraulic mounts characteristics: (a) dynamic stiffness and (b) loss angle (see online version for colours)

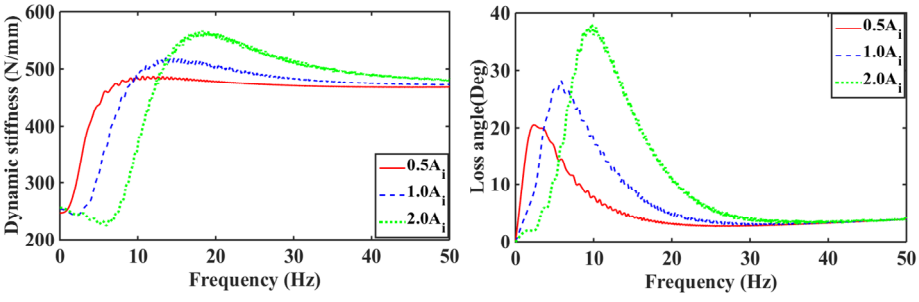

(a) (b)

Figure 4 Effect of inertia channel length L on hydraulic mounts characteristics: (a) dynamic stiffness and (b) loss angle (see online version for colours)

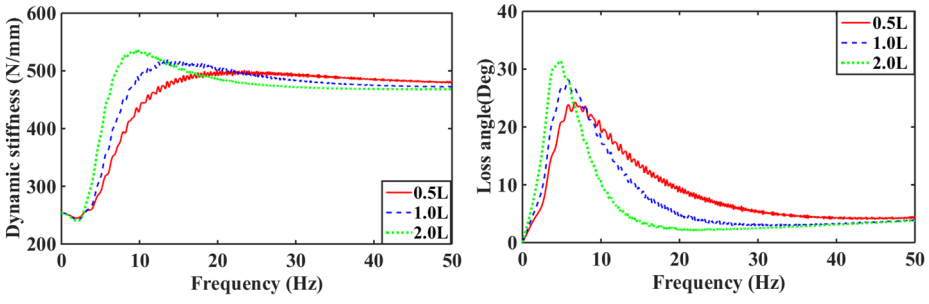

(a) (b)

Table 1 Hydraulic mounts with different configurations of inertia channels

Figure 5 Numbering of inertial channels	*Description*
C1	One inertial channel with diameter D_i , length L_i
C2	Two inertial channels with diameter D_i , 1/2 d_i and length L_i
C3	Two inertia channels with diameter 1/2 D_i , length L_i
C4	Two inertia channels with diameter D_i , length 1/2 L_i
C5	Two inertial channels with diameter D_i , length L_i and 1/2 L_i
C6	Two inertia channels with diameter D_i length L_i
C7	Three inertial channels with diameter D_i , length L_i , 1/2 L_i and 1/2 L_i
C8	Three inertial channels with diameter D_i , length L_i , L_i and 1/2 L_i
C9	Three inertial channels with diameter D_i , length L_i

C1 is a single inertia channel hydraulic mount with a cross-sectional area of D_i and a length of L_i. C2 inertia channels have di and 1/2D_i diameters, respectively, and the same length as C1. C3 inertial channels have a diameter of 1/2 D_i and the same length as C1.

C4 has two inertial channels with a length of 1/2 L_i and a cross-sectional area of D_i. The cross-sectional areas of the 2 inertial channels of C5 are both D_i, and the lengths are L_i and 1/2 L_i, respectively. The cross-sectional areas of the 2 inertial channels of the C6 structure are D_i, and the lengths of the inertial channels are all L_i. The cross-sectional areas of the 3 inertial channels of the C7 structure are all D_i, and the lengths of the inertial channels are Li, 1/2 L_i, and 1/2 L_i, respectively. The cross-sectional areas of the three inertial channels of the C8 structure are all D_i, and the lengths of the inertial channels are L_i, L_i, and 1/2 L_i. The cross-sectional areas of the three inertial channels of the C9 structure have the same inertial channel lengths as C1.

Figure 5 Multi-inertia channel hydraulic mount: (a) single inertia channel with diameter D_i , and length L_i ; (b) two inertia channels, with diameter D_i , and 1/2 D_i length L_i ; (c) two inertia channels, with diameter d_i and 1/2 D_i length L_i ; (d) two inertia channels, with diameter D_i and 1/2 L_i length; (e) two inertia channels, both with diameter D_i , and 1/2 L_i length, respectively L_i , and 1/2 L_i ; (f) 2 two inertial channels with the same structure and di length of L_i ; (g) three inertial channels, all with D_i diameter and length of L_i , 1/2 L_i ,1/2 L_i ; (h) three inertial channels, all with D_i diameter and length of L_i , L_i , 1/2 L_i and (i) three inertial channels with the same structure and d_i and the length is L_i (see online version for colours)

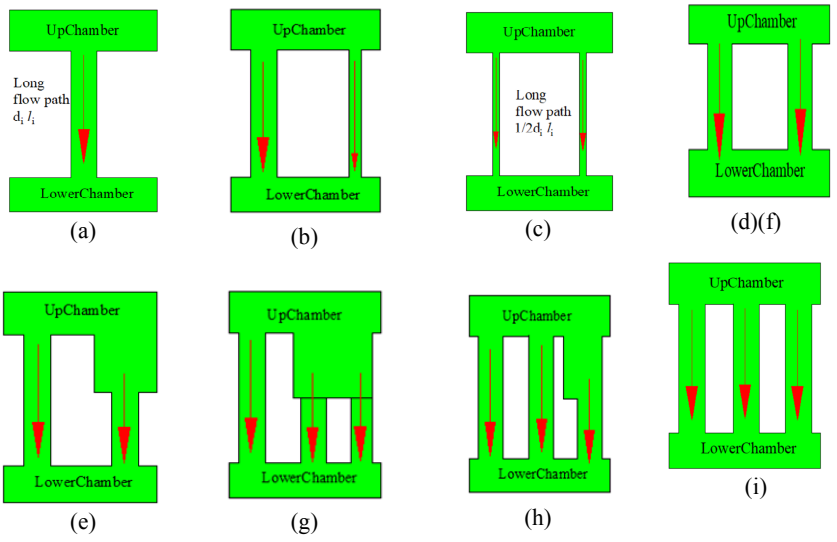

3 Multi-inertia channel hydraulic mounts frequency domain characteristics analysis

3.1 Equation derivation and verification

Singh et al. (1992) equates the set parameter model of the multi-inertia channel hydraulic mount of Figure 6(a) to the mechanical model of Figure 6(b). According to Figure 6(a), the mathematical model equation of the lumped parameters of the multi-inertia channel hydraulic mounts can be obtained as follows.

$$F_T = K_r x_e(t) + B_r \dot{x}_e(t) + A_p P_1(t) \tag{4}$$

$$P_1(t) = \frac{1}{C_u} A_p x_e(t) - \frac{\sum A_{in} x_{in}(t)}{C_u}, P_2(t) = \frac{\sum A_{in} x_{in}(t)}{C_L} \tag{5}$$

$$P_1(t) - P_2(t) = I_{in} \dot{Q}_{in}(t) + R_{in} Q_{in}(t) \tag{6}$$

$$\frac{1}{C_1}[A_p x_e(t) - \sum A_{in} x_{in}] - \frac{1}{C_2} \sum A_{in} x_{in} = I_{in} A_{in} \ddot{x}_{in} + R_{in} A_{in} \dot{x}_{in} \tag{7}$$

Figure 6 Multi-inertia channel hydraulic mount: (a) lumped parameter model and (b) equivalent mechanical model (see online version for colours)

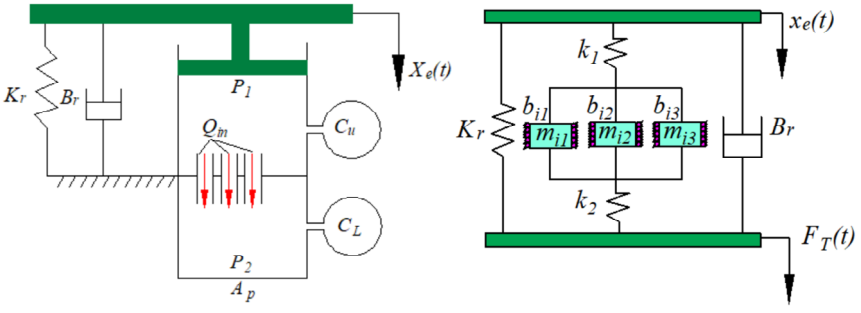

(a) (b)

Referring to Barszcz et al. (2012) and He and Singh (2005), it is known that $k_1 = A_p^2 / C_1$ is the equivalent linear stiffness of the upper chamber of the multi-inertia channel hydraulic mount, $k_2 = A_p^2 / C_2$ is the equivalent linear stiffness of the lower chamber of the multi-inertia channel hydraulic mount, b_{in} is the equivalent damping of the hydraulic mount inertia channel fluid, and $m_{in} = A_p^2 I_{in}$ is the equivalent mass of the hydraulic mount inertia channel fluid. Equations (4) and (7) can be transformed into equations (8) and (9) as follows.

$$\frac{A_p^2}{C_u}[x_e(t) - \sum x_{in}] - \frac{A_p^2}{C_L} \sum x_{in} = I_{in} A_p^2 \ddot{x}_{in} + R_{in} A_p^2 \dot{x}_{in} \ldots\ldots n = 1, 2, 3 \tag{8}$$

$$F_T = K_r x_e(t) + B_r \dot{x}_e(t) + \frac{A_p^2}{C_u}[x_e - \sum x_{in}] \tag{9}$$

Due to $C_L \gg C_u$ in hydraulic mounts and (Barszcz et al., 2012; Vahdati, 2005), the mounts are at low frequencies (1–50 Hz) $B_r = 0$. Thus, the equivalent inertia and equivalent fluid resistance of the inertia channel and equation (8) is simplified to equation (10).

$$k_1[x_e(t) - \sum x_{in}] = m_{in} \ddot{x}_{in} + b_{in} \dot{x}_{in} \tag{10}$$

where

$$I_{eq} = \frac{\Pi_{i=1}^{n} I_{i,i}}{\sum_{i=1}^{n} \binom{R_{i,i}}{n\text{-}1}} \Leftrightarrow m_{eq} = A_p^2 I_{eq}, R_{eq} = \frac{\Pi_{i=1}^{n} R_{i,i}}{\sum_{i=1}^{n} \binom{R_{i,i}}{n\text{-}1}} \Leftrightarrow b_{eq} = A_p^2 R_{eq}$$

Equations (9) and (10) can be further simplified to equations (11) and (12).

$$k_1[x_e(t) - x_{eq}(t)] = m_{eq}\ddot{x}_{eq}(t) + b_{eq}\dot{x}_{eq}(t) \tag{11}$$

$$F_T = K_r x_e(t) + k_1[x_e(t) - x_{eq}(t)] \tag{12}$$

For equations (11) and (12) Laplace transformations see equation (13).

$$K_{22}(s) = \frac{F_T(s)}{x_e(s)} = \frac{(K_r + k_1)\left[m_{eq}s^2 + b_{eq}s + \dfrac{K_r k_1}{K_r + k_1}\right]}{m_{eq}s^2 + b_{eq}s + k_1} \tag{13}$$

Organising equation (13) into a standard second-order system.

$$K_{22}(s) = \frac{(K_r + k_1)[s^2 + 2\xi_1\omega_1 s + \omega_1^2]}{s^2 + 2\xi_2\omega_2 s + \omega_2^2} \tag{14}$$

where

$$\omega_1 = \sqrt{\frac{K_r k_1}{(K_r + k_1) I_{eq} A_p^2}} \quad , \quad \omega_2 = \sqrt{\frac{k_1}{I_{eq} A_p^2}} \quad , \quad \xi_1 = \frac{R_{eq}}{2}\sqrt{\frac{(K_r + k_1)A_p^2}{K_r k_1 I_{eq}}} \quad ,$$

$$\xi_2 = \frac{R_{eq}}{2}\sqrt{\frac{A_p^2}{k_1 I_{eq}}}$$

Singh et al. (1992) can represent equations (4)–(6) in the form of a block diagram, where the blue dashed box is the hydraulic transfer path and the red dashed line is the rubber transfer path, as shown in Figure 7.

According to Figure 7, the closed-loop transfer function of the system under external excitation of the multi-inertia channel hydraulic mount is obtained as follows:

$$K_{33}(s) = \frac{F_T}{x_e}(s) = \frac{K_r(A_3 s^3 + A_2 s^2 + A_1 s + A_0) + A_p^2(B_3 s^3 + B_2 s^2 + B_1 s + B_0)}{A_3 s^3 + A_2 s^2 + A_1 s + A_0} \tag{15}$$

where

$$A_3 = I_1 I_2 C_u C_L, A_2 = C_u C_L I_1 R_2 + C_u C_L I_2 R_1$$
$$A_1 = C_u C_L R_1 R_2 + C_u I_1 + C_u I_2, A_0 = C_u R_1 + C_u R_2 + C_L I_1 + C_L I_2 + C_L R_1 + C_L R_2$$
$$B_3 = C_L I_1 I_2, B_2 = C_L I_1 R_2 + C_L I_2 R_1, B_1 = C_L R_1 R_2 + I_1 + I_2, B_0 = R_1 + R_2$$

The dynamic stiffness $K_{22}(s)$ solved by the equivalent mechanical mathematical model is compared numerically with the dynamic stiffness $K_{33}(s)$ of the multi-inertia channel hydraulic mount solved by the square diagram of Singh et al. (1992) to validate the developed mathematical model of the multi-inertia channel hydraulic mount. The equivalent mechanical mathematical model is calculated to obtain the dynamic stiffness

$K_{22}(s)$ and the dynamic stiffness $K_{33}(s)$ of the multi-inertia channel hydraulic mounts solved by the block diagram as shown in Figure 8. The curves of $K_{22}(s)$ and $K_{33}(s)$ in Figure 8 are the same. Therefore, it is proved that the mathematical model solved for the dynamic stiffness $K_{22}(s)$ is correct.

Figure 7 Multi-inertia channel hydraulic mount cube diagram (see online version for colours)

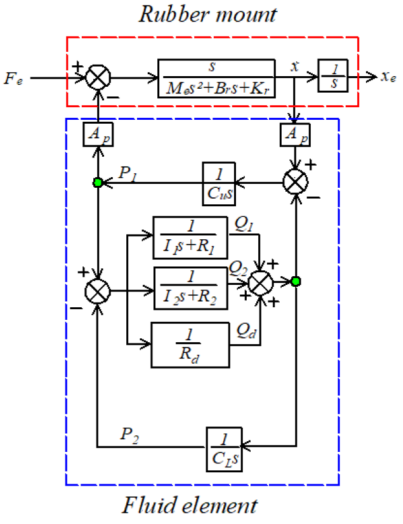

Source: Singh et al. (1992)

Figure 8 Dynamic characteristics of multi-inertia channel hydraulic mounts: (a) dynamic stiffness and (b) loss angle (see online version for colours)

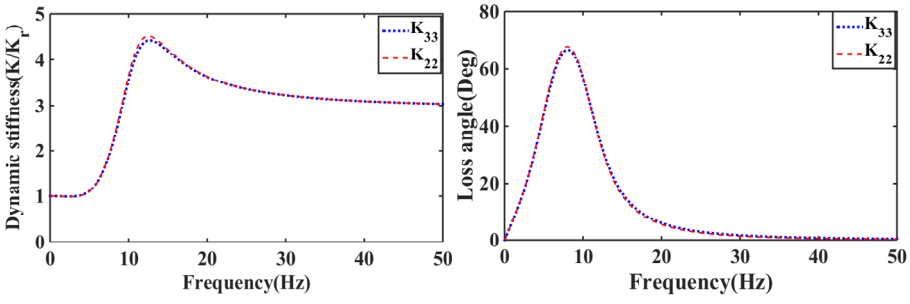

(a) (b)

3.2 Multi-inertia channel hydraulic mounts frequency domain characteristics analysis

1 To analyse the effect of changes in the number and length of inertia channels on the characteristics of the hydraulic mount and to compare the changes in the mounts characteristics of the three structures C1, C4, and C6.

2 To analyse the effect of changes in the number of inertia channels and cross-sectional area on the characteristics of the hydraulic mount and to compare the changes in the mounts characteristics of the three structures C1, C2, and C3.

3 To analyse the effect of changes in the number of long inertia channels on the characteristics of the hydraulic mount and to compare the changes in the mounts characteristics of the three structures C1, C6, and C9.

4 Analysis of the effect of short inertia channel changes on hydraulic mounts characteristics when the number of inertia channels is greater than 2, and comparison of the changes in mounts characteristics of four structures C5, C6, C7, and C8.

5 To analyse the effect of the number of short inertia channels on the characteristics of the hydraulic mount when the number of inertia channels is constant, the changes in the mounts characteristics of the three structures C7, C8, and C9 are compared.

It can be seen in Figure 9(a) that the peak and peak frequencies of dynamic stiffness and loss angle of hydraulic mounts increase with the number of inertia channels for the same inertia channel cross-sectional area. Figure 9(b) shows that adding a 1/2Di inertia channel to the existing inertia channel has less effect on the dynamic characteristics of the hydraulic mounts. However, the sum of the cross-sectional area of the two inertial channels C3 is the same as that of C1 but exhibits a larger stiffness and loss angle at low frequencies. It can be seen that the reduced cross-sectional area of the inertia channel hydraulic mounts exhibits greater stiffness and damping at lower frequencies. Figure 9(c) shows that increasing the number of long inertia channels can achieve suspended broadband vibration isolation, which is the same conclusion as in Zhang and Shangguan (2006). Figure 9(d) shows that the number of inertia channels increases under the same conditions as the total inertia channel length of the hydraulic mounts and the peak dynamic stiffness and loss angle of the hydraulic mounts with long and short inertia channels increase on the basis of the hydraulic mounts with long and short inertia channels. Figure 9(e) shows that increasing the number of short inertia channels can achieve broadband tuning. Therefore, the number, cross-sectional area, and length of the different inertia channels directly affect the dynamic characteristics of the hydraulic mounts.

4 Multi-inertia channel hydraulic mounts time domain characteristics analysis

Although, multi-inertia channel bushing time-domain characteristics have been reported in Chai et al. (2013, 2014). However, differences between hydraulic mounts and hydraulic bushings have been demonstrated in Yang et al. (2015). In this section, the time domain characteristics of the multi-inertia channel hydraulic mounts are studied and analysed by recombining equation (13) as shown in equation (16) below.

$$K_{22}(s) = K_{hr} + K_{hy} = K_r + k_1 \frac{s(s+\lambda)}{s^2 + 2\xi_2\omega_2 s + \omega_2^2} \tag{16}$$

where

$$\omega_2 = \sqrt{\frac{k_1}{I_{eq}A_p^2}}, \xi_2 = \frac{R_{eq}}{2}\sqrt{\frac{A_p^2}{k_1 I_{eq}}}, \lambda = \frac{R_{eq}}{I_{eq}}$$

Figure 9 Dynamic stiffness and loss angle of multi-inertia channel hydraulic mounts: (a) C1, C4, C6; (b) C1, C2, C3; (c) C1, C6, C9; (d) C5, C6, C7, C8 and (e) C7, C8, C9 (see online version for colours)

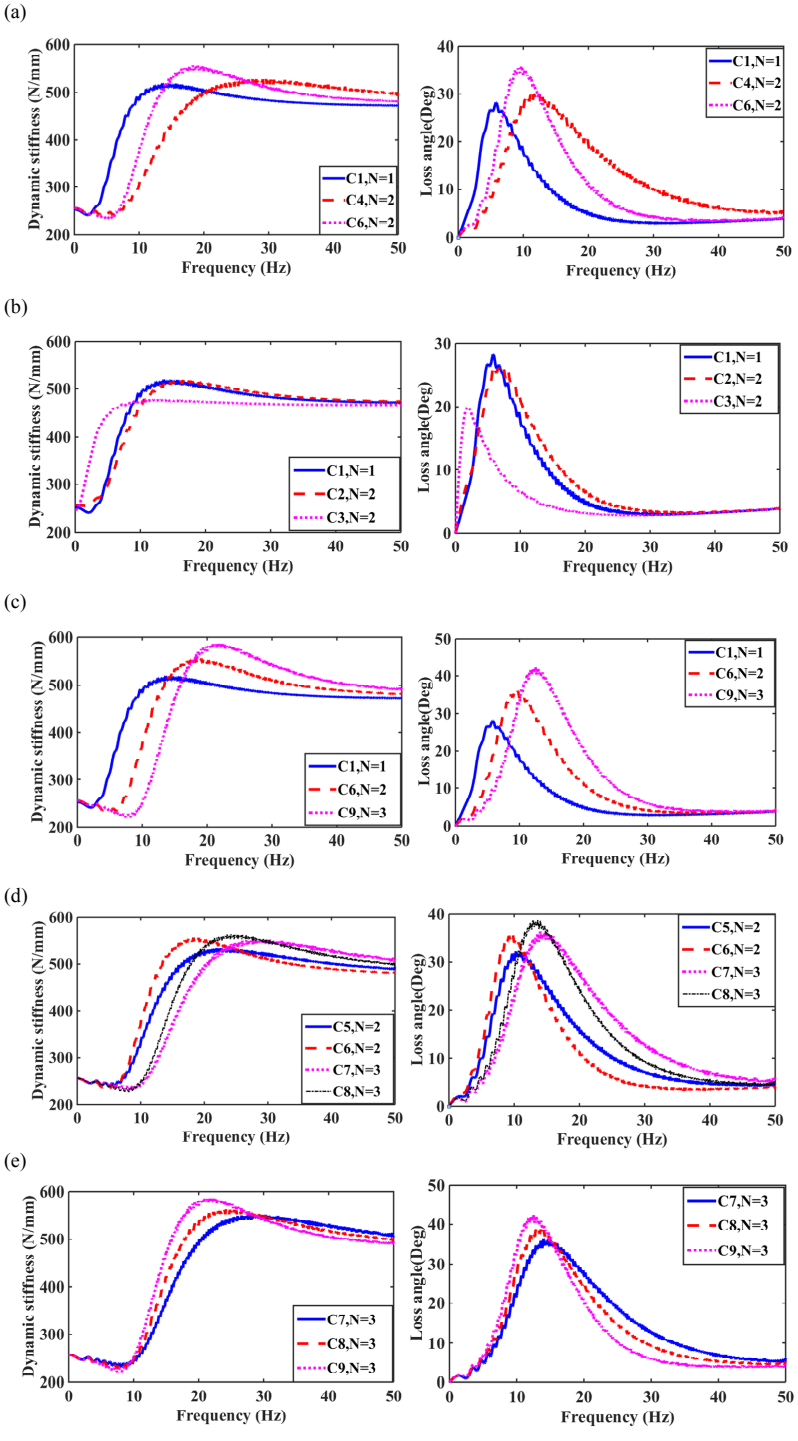

4.1 Sinusoidal excitation

In order to facilitate the solution of the transmitted forces for the sine excitation $x(t) = A\sin\omega t$ multi-inertia channel hydraulic mounts, equation (16) is appropriately rearranged to equation (17). Where the transmitted force of the rubber part is expressed as $F_{Th}(t)$ and the transmitted force of the hydraulic part is $F_{Th}(t)$. In this case, the hydraulic transmitted forces for solving the multi-inertia channel hydraulic mounts are solved by the method of Chai et al. (2014), using the input excitation $x(t)$ and the hydraulic part stiffness $F_{Thy}(t)$ for the convolution solution. The specific solution is as follows:

$$K_{22}(s) = K_r + k_1\left[1 - \frac{\omega_2^2}{s^2 + 2\xi_2\omega_2 s + \omega_2^2} - \frac{(2\xi_2\omega_2 - \lambda)s}{s^2 + 2\xi_2\omega_2 s + \omega_2^2}\right] \tag{17}$$

$$\begin{aligned} K_{hy}(t) &= k_1 L^{-1}\left(1 - \frac{\omega_2^2}{s^2 + 2\xi_2\omega_2 s + \omega_2^2} - \frac{(2\xi_2\omega_2 - \lambda)s}{s^2 + 2\xi_2\omega_2 s + \omega_2^2}\right) \\ &= \left[\delta(t) - \frac{\omega_2(t)}{\sqrt{1-\xi_2^2}} e^{-\xi_2\omega_2 t}\sin(\omega_d t) + \frac{2\xi_2\omega_2(t) - \lambda}{\sqrt{1-\xi_2^2}} e^{-\xi_2\omega_2 t}\sin(\omega_d t - \theta)\right] \end{aligned} \tag{18}$$

$$F_{Thr}(t) = K_r x(t) \tag{19}$$

$$F_{Thy}(t) = K_{hy}(t) * x(t) = \int_0^t K_{hy}(\tau)x(t-\tau)\mathrm{d}\tau \tag{20}$$

where

$$\omega_d = \omega 2\sqrt{1-\xi_2^2}\ ,\ \theta = \tan-(\sqrt{1-\xi_2^2}\ /\ \xi_2)$$

According to the above equations, the time domain response of the C1 structure with hydraulic mounts at 10 Hz and 30 Hz excitation frequency and 0.3 mm amplitude is solved. Comparing the calculated transmitted forces in Figure 8(a) and (b) with the results of the constructed AMEsim model, a good agreement can be observed. $F_{Th}(t)$ the error between the peak calculated by the mathematical model and the peak of the model built by AMEsim is about 6.26% at 10 Hz and about 2.07% at 30 Hz. Differences between the mathematical calculations and the AMEsim model could be due to differences between the equivalent damping at different frequencies.

4.2 Step excitation

Step response $x(t) = Au(t)$, combined with equation (16) yields the transmitted force $F_{thr}(t)$ for the rubber part and $F_{thy}(t)$ for the hydraulic part. Where the method for solving the hydraulic part of the transmitted force is the same as that in Section 4.1 using the convolution method of Chai et al. (2014), which is solved as follows.

$$F_{Thr}(t) = K_r x(t) \tag{21}$$

$$F_{Thy}(t) = K_{hy}(t) * x(t) = \int_0^t K_{hy}(\tau)x(t-\tau)\mathrm{d}\tau = k_1 \frac{A}{\omega_d} e^{-\kappa t}(\kappa \sin \omega_d t + \omega_d \cos \omega_d t)$$
$$-Ak_1 \frac{2\xi 2\omega 2 - \lambda}{\omega d\, \omega 2}\{e^{-\kappa t}[\kappa \sin(\omega_d t - \theta) + \omega_d \cos(\omega_d t - \theta)] + \kappa \sin\theta - \omega d \cos\theta\} \quad (22)$$

where

$$\kappa = \omega_2 \xi_2$$

Combining equations (21) and (22) to solve for the time domain response of the Fth(t) under step response excitation of C1 hydraulic mounts. Figure 11 shows the comparison between the mathematical model and the AMEsim model, and there is a good agreement between the two models. From Figure 11(a) and (b), it can be seen that the error between the peaks of the models built by the two methods is about 12.7% at the excitation amplitude A = 0.3 mm and the maximum peak difference is about 8.62% at the excitation amplitude A = 3 mm.

Figure 10 Transferred force of C1 structure hydraulic mount: (a) f = 10 Hz, A = 0.3 mm and (b) f = 30 Hz, A = 0.3 mm (see online version for colours)

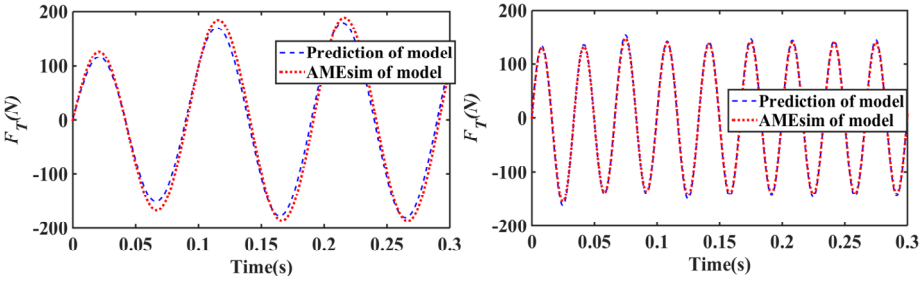

Figure 11 Transferred force of hydraulic mount of C1 structure: (a) A = 0.3 mm and (b) A = 3mm (see online version for colours)

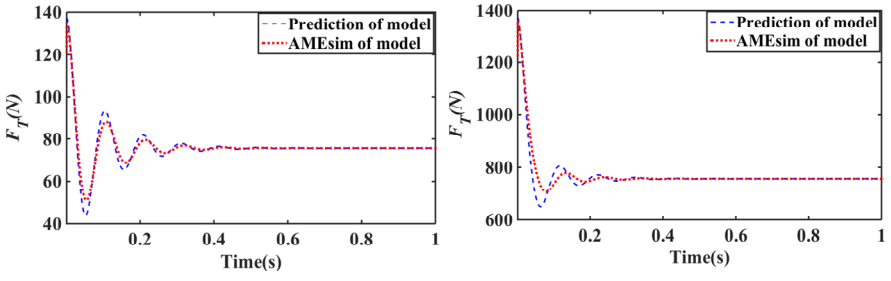

Figure 12 investigates the effect of equivalent damping R_{eq} and inertia I_{eq} on the transmitted force under step-response excitation, with R_{eq} and I_{eq} values (adjusted by varying the length L_i or cross-sectional area A_i) having a significant effect on the peak amplitude and period $t_d = 2\pi/\omega_d$ of the oscillation. When the value of I_{eq} increases, both t_d and the peak transmitted force increase, and the overshoot of the system also

increases, as shown in Figure 12(a). Because increasing I_{eq} when R_{eq} is constant From equation (14) we can get ω_2 and ξ_2 both increase, $e^{-\kappa t}$ combined with equation (22) we can see that the decay exponent decreases. As shown in Figure 12(b), the increase in the equivalent damping R_{eq} significantly reduces the amplitude of the system oscillation and increases the $e^{-\kappa t}$ value. It can be concluded that different lengths and cross-sectional areas can be combined in making the multi-inertia channel hydraulic mounts exhibit the best vibration isolation performance.

Figure 12 Effect of equivalent damping R_{eq} and inertia I_{eq} on transient transmitted force for step response hydraulic mounts: (a) effect of equivalent inertia I_{eq} on transmitted force for hydraulic mounts and (b) effect of equivalent damping R_{eq} on transmitted force for hydraulic mounts (see online version for colours)

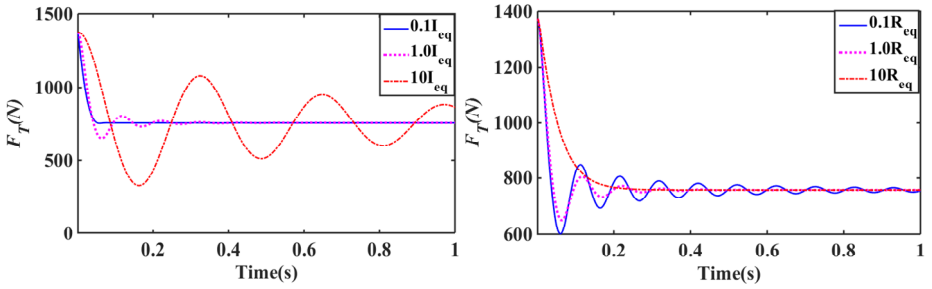

Figure 13 shows the variation of hydraulic mounts transfer force for the same step response excitation for 5 combinations of 9 inertia channels proposed in this paper.

Figure 13(a) shows that the RMS values of C1, C4, and C6 transfer forces are 772.5093N, 764.6361N, and 765.9450N, respectively. This shows that the C4 structure with hydraulic mount has the best vibration isolation performance. Meanwhile, the overshoot of C1 is minimal. Because, the damping ratio $\xi_{2\text{-}C1} = 0.154$ of the C1 structure is greater than the damping ratio $\xi_{2\text{-}C4} = 0.077$ of C4 and the damping ratio $\xi_{2\text{-}C6} = 0.1090$ of C6.

Figure 13(b) shows that the RMS values of C1, C2, and C3 transfer forces are 772.5093 N, 777.6950 N, and 799.5279 N, respectively, which shows that C1 has the smallest RMS for the same step response. It can be seen that the parallel connection of a smaller cross-sectional area inertia channel to the C1 inertia channel can improve the vibration isolation performance of the hydraulic mounts. Although there is almost no overshoot in C3, the RMS of the transfer force in C3 is the largest. It can be seen that increasing the number of inertia channels with the same total cross-sectional area of the hydraulic mounts increases the damping of the mounts. However, the vibration isolation performance of the mounts is reduced.

Figure 13(c) shows that C1, C6 and C9 transfer force RMS values are 772.5093 N, 765.9450 N and 763.8864 N, respectively, and C9 has the smallest transfer force RMS for the same step response. Meanwhile, C9 has the largest overshoot and oscillation period. It can be seen that the damping ratio ξ_2 of the hydraulic mounts decreases as the

number of inertia channels n increases, and the damped self-oscillation angular frequency ω_d increases.

Figure 13 Step response system transmitted force variation for multi-inertia channel hydraulic mounts: (a) C1, C4, C6 combination; (b) C1, C2, C3 combination; (c) C1, C6, C9 combination; (d) C5, C6, C7, C8 combination and (e) C7, C8, C9 combination (see online version for colours)

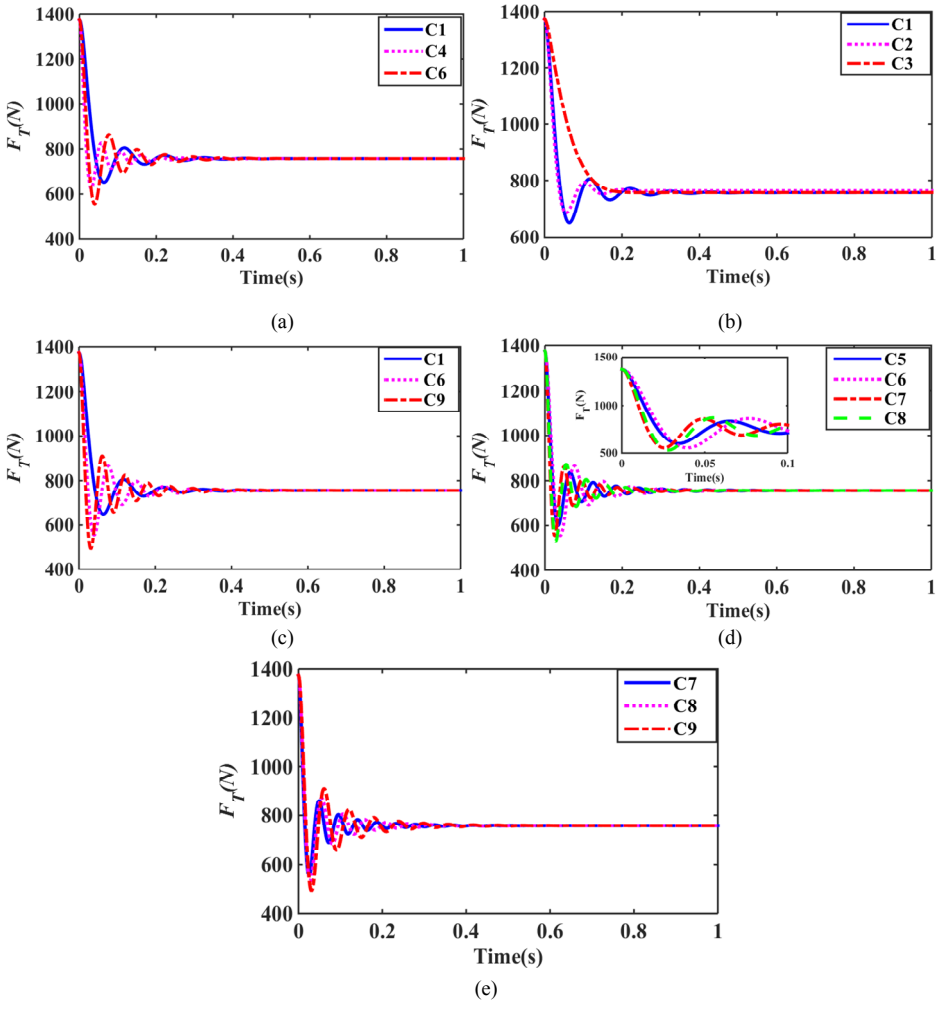

Figure 13(d) shows that the RMS values of C5, C6, C7, and C8 transfer forces are 765.2990 N, 765.9450 N, 762.8364 N, and 763.1861, respectively. It can be seen that C5 and C7 have the smallest RMS of transfer force for the same step response. Therefore, increasing the number of inertia channels can improve the hydraulic mounts' vibration isolation performance.

Figure 13(e) shows that the RMS values of transfer forces for C7, C8, and C9 are 762.8364 N, 763.1861 N, and 763.8864 N, respectively, and C7 has the smallest RMS

value. For the same number of inertia channels, increasing the number of short inertia channels can improve the vibration isolation performance of hydraulic mounts.

4.3 Random pavement excitation

Figure 14 shows a 1/4 car model with a multi-inertia channel hydraulic mount. The model includes an engine, hydraulic mount, vehicle frame, suspension, and tyres. Where K_u and B_u denote suspension stiffness and damping, K_t is tyre stiffness; engine excitation $F_{exc}(t)$, road input $h(t)$, $x_e(t)$, $y_c(t)$ and $z_w(t)$ denote engine displacement, vehicle frame displacement, and under-suspension unsprung displacement, respectively. Thus, the mathematical expression for building a 1/4 car model with multi-inertia channel hydraulic mount is shown in equation (23).

$$\begin{cases} M_e\ddot{x}_e + K_r(x_e - y_c) + B_r(\dot{x}_e - \dot{y}_c) + F = F_{exc} \\ M_b\ddot{y}_c - K_r(x_e - y_c) + B_r(\dot{x}_e - \dot{y}_c) + K_u(y_c - z) + B_u(\dot{y}_c - \dot{z}) - F = 0 \\ M_w\ddot{z} - K_u(y_c - z) - B_u(\dot{y}_c - \dot{z}) + K_t(z - h) = 0 \end{cases} \tag{23}$$

The road input model plays an important role in vehicle dynamics analysis for a more realistic reflection of the effect of external excitation on different inertia channels. The power spectral density of the pavement can be obtained by using the power spectral density (PSD) based longitudinal random pavement unevenness classification proposed by ISO 8608 (Yang, 2016) whose solution expression is shown in equation (24). Where, the single-wheel continuous vibration pavement input signal of a car driving on a Class C road surface is shown in Figure 15.

$$G_q(n) = G_q(n_0)\left(\frac{n}{n_0}\right)^{-\omega} \tag{24}$$

where n is the spatial frequency in m^{-1}; n_0 is the reference spatial frequency, $n_0 = 0.1\,\mathrm{m}^{-1}$; $G_q(n)$ is the road surface spectrum value at the reference spatial frequency, generally known as the unevenness value of the road surface, in $\mathrm{m}^2/\mathrm{m}^{-1}$; ω is the frequency index.

Figure 14 Multi-inertia channel hydraulic mount 1/4 car model (see online version for colours)

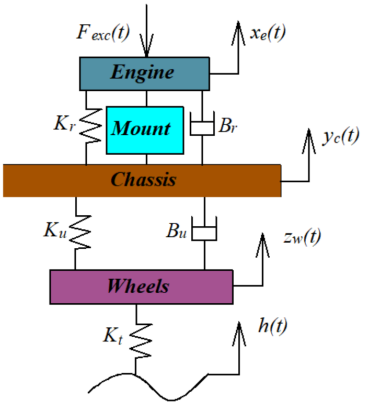

Figure 15 Single wheel continuous vibration road input signal (see online version for colours)

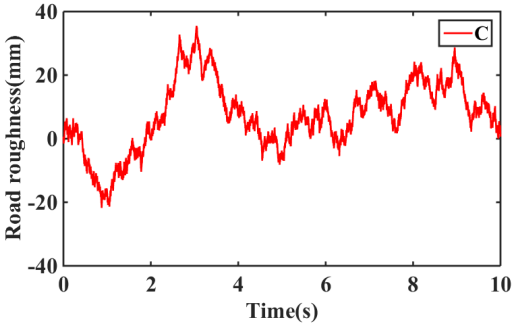

Figure 16 numerically calculates the root mean square (RMS) T_a of the engine end acceleration and vehicle end acceleration transmissibility and the RMS T_{xe-yc} of the relative engine and vehicle displacement transmissibility for each of the nine inertia channels in five combinations on Class C roads.

Figure 16(a) shows that the RMS values of T_a in C1, C4, and C6 are 39.2066, 26.3253, and 29.1892, respectively, and the RMS values of T_{xe-yc} are 0.4927, 0.7309, and 0.6334. It can be seen that increasing the number of inertia channels decreases the T_a RMS and increases the T_{xe-yc} RMS with constant inertia channel cross-sectional area, and short inertia channels have a greater effect on the system.

Figure 16(b) shows that the RMS values of T_a in C1, C2, and C3 are 39.2066, 36.2033, and 30.9796, respectively, and the RMS values of T_{xe-yc} are 0.4927, 0.5352, and 0.2565. It can be concluded that adding small cross-sectional area inertia channels with the same cross-sectional area of existing inertia channels will decrease the T_a value and increase the T_{xe-yc} value. However, increasing the number of inertia channels with the same total cross-sectional area increases the RMS value of T_a and decreases the RMS value of T_{xe-yc} for hydraulic mounts.

Figure 16(c) shows that the RMS values of T_a in C1, C6, and C9 are 39.2066, 29.1892, and 26.9823, and the RMS values of T_{xe-yc} are 0.4927, 0.6334, and 0.6973, respectively. Increasing the number of inertias directly affects the engine-to-vehicle frame acceleration transmissibility and the relative engine-to-vehicle displacement transmissibility.

Figure 16(d) shows that the RMS values of T_a in C5, C6, C7, and C8 are 27.2524, 29.1892, 25.4610, and 25.9575, respectively, and the RMS values of T_{xe-yc} are 0.6910, 0.6334, 0.7610 and 0.7343. It can be seen that the same inertia channel cross-sectional area and short inertia channel will reduce the low-frequency large amplitude vibration isolation performance of hydraulic mounts.

Figure 16(e) shows that the RMS values of T_a in C7, C8, and C9 are 25.4610, 25.9575, and 26.9823, respectively, and the RMS values of T_{xe-yc} are 0.7610, 0.7343, and 0.6973. The C9 structure hydraulic mount has the best low-frequency large-amplitude vibration isolation performance, and the C7 structure hydraulic mount has the worst low-frequency large-amplitude vibration isolation performance. It can be seen that the low-frequency large-amplitude vibration isolation performance of hydraulic mounts

decreases when the number of short inertia channels increases with the same number of inertia channels.

Figure 16 Multi-inertia channel hydraulic mount vibration accelerations and relative bit transmissibility for: (a) C1, C4, C6; (b) C1, C2, C3; (c) C1, C6, C9; (d) C5, C6, C7, C8 and (e) C7, C8, C9 (see online version for colours)

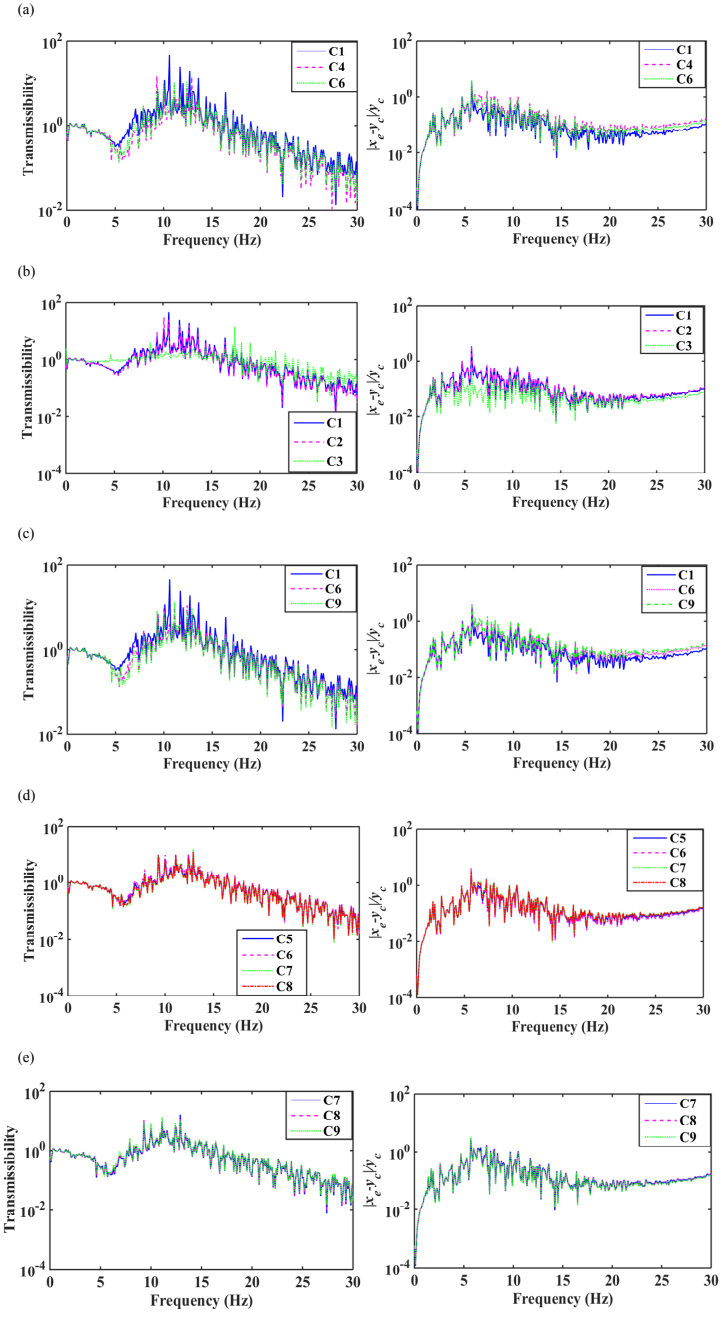

By analysing the results of the 1/4 car model with multi-inertia channel hydraulic mounts it is obtained that:

1 Under the condition of the constant cross-sectional area of the inertia channel, increase the number of inertia channels, hydraulic mounts with low frequency large amplitude vibration isolation performance decreases.

2 The total inertia channel cross-sectional area of the hydraulic mounts remains the same and increasing the number of inertia channels can improve the low-frequency large-amplitude vibration isolation performance of the hydraulic mounts.

3 Increasing the number of short inertia channels with the same number of inertia channels will reduce the low-frequency large amplitude vibration isolation performance of the hydraulic mounts.

5 Conclusion

The paper investigates the effects of variations in the number and length of inertia channels and cross-sectional area on the low-frequency dynamic characteristics of hydraulic mounts. Firstly, the high and low-frequency characteristics were analysed by combining hydraulic mounts with inertial and decoupler membrane channels. Secondly, to observe the effects of different inertia channel cross-sectional area and length variations on the dynamic stiffness and hysteresis angle of the hydraulic mounts. And then, nine different structures of inertia channels are proposed; the equivalent mechanical method is used to obtain the mathematical model of hydraulic mounts, and the correctness of the model is verified by comparison with the block diagram method proposed by Singh et al. (1992). Next, the influence of the number and length of inertia channels and the variation of the cross-sectional area on the low-frequency dynamic characteristics of the hydraulic mounts is analysed based on the mathematical model. Finally, the hydraulic mounts system model of the 1/4 vehicle model is built to analyse the effect of different inertia channels on the mount's vibration isolation performance under road excitation.

The results show that

1 the vibration isolation performance of the hydraulic mounts at low frequencies relies mainly on inertia channel action

2 the structural parameters of the inertia channel of the hydraulic mounts directly affect the dynamic characteristics of the mounts.

At the same time, increasing the number of inertia channels can broaden the low-frequency dynamic characteristics of the hydraulic mounts.

Funding

Sanming University introduced high-level talents scientific research start-up funding (project number: 23YG01).

References

Barszcz, B., Dreyer, J.T. and Singh, R. (2012) 'Experimental study of hydraulic engine mounts using multiple inertia tracks and orifices: narrow and broad band tuning concepts', *Journal of Sound and Vibration*, Vol. 331, No. 24, pp.5209–5223.

Chai, T., Dreyer, J.T. and Singh, R. (2014) 'Time domain responses of hydraulic bushing with two flow passages', *Journal of Sound and Vibration*, Vol. 333, No. 3, pp.693–710.

Chai, T., Dreyer, J.T. and Singh, R. (2015) 'Frequency domain properties of hydraulic bushing with long and short passages: system identification using theory and experiment', *Mechanical Systems & Signal Processing*, Vols. 56–57, pp.92–108.

Chai, T., Singh, R. and Dreyer, J.T. (2013) *Dynamic Stiffness of Hydraulic Bushing with Multiple Internal Configurations*, Sae Technical Paper, 2013-01-1924.

Fan, R., Fei, Z., Zhou, B., Gong, H. and Song, P. (2020) 'Two-step dynamics of a semiactive hydraulic engine mount with four-chamber and three-fluid-channel', *Journal of Sound and Vibration*, Vol. 480, p.115403.

He, S. and Singh, R. (2005) 'Estimation of amplitude and frequency dependent parameters of hydraulic engine mount given limited dynamic stiffness measurements', *Noise Control Engineering Journal*, Vol. 53, No. 6, pp.271–285(15).

ISO I. 8608 (2016) Mechanical Vibration-Road Surface Profiles-Reporting of Measured Data, BSI Standards Publication, London, UK.

Li, Y., Jiang, J.Z. and Neild, S.A. (2019) 'Optimal fluid passageway design methodology for hydraulic engine mounts considering both low and high frequency performances', *Journal of Vibration and Control,* pp.2749–2757, 5(21-22.

Lu, M. and Ari-Gur, J. (2002) 'Study of hydromount and hydrobushing with multiple inertia tracks', *JSAE Annual Congress Proceedings*, Vol. 2002, pp.68–02.

Singh, R., Kim, G. and Ravindra, P.V. (1992) 'Linear analysis of automotive hydro-mechanical mount with emphasis on decoupler characteristics', *Journal of Sound and Vibration*, Vol. 158, No. 2, pp.219–243.

Tiwari, M., Adiguna, H. and Singh, R. (2003) 'Experimental characterization of a nonlinear hydraulic engine mount', *Noise Control Engineering Journal*, Vol. 51, No. 1, pp.212–223.

Türkücü, T. and Keleş, Ö. (2018) 'Magneto-rheological engine mount design and experimental characterization', *Journal of Mechanical Science and Technology*, Vol. 32, No. 11, pp.5171–5178.

Vahdati, N. (2005) 'Double-notch single-pumper fluid mounts', *Journal of Sound and Vibration*, Vol. 285, No. 3, pp.697–710.

Yang, C., Yin, Z., Zhaoping, L., Duan, X. and Shangguan, W. (2016a) 'Experiment and calculation of the low frequency performance of a hydraulic bushing with multiple tracks', *Journal of Vibration Measurement and Diagnosis*, Vol. 36, No. 6, pp.1057–1064.

Yang, C.F., Yin, Z.H., Shangguan, W.B. and Duan, X.P. (2016b) 'A study on the dynamic per-formance for hydraulically damped rubber bushings with multiple inertia tracks and ori-fices: parameter identification and modeling', *Shock and Vibration*, Vol. 2016, p.3695950.

Yang, C.F., Yin, Z.H., Wu, C.Y. and Shangguan, W.B. (2015) 'Comparison of working mechanisms of hydraulic damped bushings and hydraulic engine mounts', *Journal of South China University of Technology (Natural Science Edition)*, Vol. 43, No. 08, pp.82–90.

Yoon, J. and Singh, R. (2010a) 'Dynamic force transmitted by hydraulic mount: estimation in frequency domain using motion and/or pressure measurements and quasi-linear models', *Noise Control Engineering Journal*, Vol. 58, No. 4, pp.403–419.

Yoon, J.Y. and Singh, R. (2010b) 'Indirect measurement of dynamic force transmitted by a nonlinear hydraulic mount under sinusoidal excitation with focus on super-harmonics', *Journal of Sound and Vibration*, Vol. 329, No. 25, pp.5249–5272.

Yu, Y., Naganathan, N.G. and Rao, V.D. (2001) 'Literature review of automotive vehicle engine mounting systems', *Mechanism and Machine Theory*, Vol. 36, No. 1, pp.123–142.

Zhang, Y.Q. and Shangguan, W.B. (2006) 'A novel approach for lower frequency performance design of hydraulic engine mounts', *Computers and Structures*, Vol. 84, Nos. 8–9, pp.572–584.

Appendix

Symbol	*Name*	*Value*	*Symbol*	*Name*	*Value*
K_r	Rubber Stiffness	2.5×10^5 N/m	L	Inertia channel length	100 mm
B_r	Rubber damping	100 N.s/m	A_i	Cross-sectional area of the inertia channel	$3 \times 10^{-5}m^2$
A_p	Equivalent cross-sectional area of the upper chamber	$2.5 \times 10^{-3}m^2$	η	Fluid viscosity	0.06 pa.s
C_u	Upper chamber volume flexibility	$3.0 \times 10^{-11}m^5/N$	I_d	Fluid inertia in decoupler	7.5×10^4 kg/m^4
C_L	Flexibility of the lower chamber volume	$2.6 \times 10^{-9}m^5/N$	R_d	Linear fluid resistance in decoupler	1.17×10^7 kg/(s.m^4)